Cellular/Molecular

Mitochondria Maintain Distinct Ca^{2+} Pools in Cone Photoreceptors

Michelle M. Giarmarco,[1]* Whitney M. Cleghorn,[1]* Stephanie R. Sloat,[1] James B. Hurley,[1,2] and Susan E. Brockerhoff[1,2]

[1]Department of Biochemistry and [2]Department of Ophthalmology, University of Washington, Seattle, Washington 98109

Ca^{2+} ions have distinct roles in the outer segment, cell body, and synaptic terminal of photoreceptors. We tested the hypothesis that distinct Ca^{2+} domains are maintained by Ca^{2+} uptake into mitochondria. Serial block face scanning electron microscopy of zebrafish cones revealed that nearly 100 mitochondria cluster at the apical side of the inner segment, directly below the outer segment. The endoplasmic reticulum surrounds the basal and lateral surfaces of this cluster, but does not reach the apical surface or penetrate into the cluster. Using genetically encoded Ca^{2+} sensors, we found that mitochondria take up Ca^{2+} when it accumulates either in the cone cell body or outer segment. Blocking mitochondrial Ca^{2+} uniporter activity compromises the ability of mitochondria to maintain distinct Ca^{2+} domains. Together, our findings indicate that mitochondria can modulate subcellular functional specialization in photoreceptors.

Key words: calcium; mitochondria; mitochondrial uniporter; photoreceptor; zebrafish

Significance Statement

Ca^{2+} homeostasis is essential for the survival and function of retinal photoreceptors. Separate pools of Ca^{2+} regulate phototransduction in the outer segment, metabolism in the cell body, and neurotransmitter release at the synaptic terminal. We investigated the role of mitochondria in compartmentalization of Ca^{2+}. We found that mitochondria form a dense cluster that acts as a diffusion barrier between the outer segment and cell body. The cluster is surprisingly only partially surrounded by the endoplasmic reticulum, a key mediator of mitochondrial Ca^{2+} uptake. Blocking the uptake of Ca^{2+} by mitochondria causes redistribution of Ca^{2+} throughout the cell. Our results show that mitochondrial Ca^{2+} uptake in photoreceptors is complex and plays an essential role in normal function.

Introduction

Vertebrate retinal photoreceptors are specialized neurons that initiate vision by transducing light into an electrical signal. These highly polarized cells are composed of three physiologically discrete regions: the outer segment containing phototransduction machinery, the cell body where proteins are synthesized and trafficked, and the synapse that releases neurotransmitter onto downstream neurons (Dowling, 1987).

Received Aug. 24, 2016; revised Jan. 10, 2017; accepted Jan. 12, 2017.

Author contributions: M.M.G., W.M.C., J.B.H., and S.E.B. designed research; M.M.G. and W.M.C. performed research; M.M.G., W.M.C., S.R.S., J.B.H., and S.E.B. analyzed data; M.M.G., W.M.C., J.B.H., and S.E.B. wrote the paper.

This work was supported by the National Science Foundation (GRFP Grant 2013158531 to M.M.G.) and the National Institutes of Health (National Eye Institute Grants 5T32EY007031 to W.M.C. and M.M.G. and EY026020 to J.B.H. and S.E.B.). We thank Ed Parker for generating serial block-face scanning electron microscopy images, Ralph Nelson for guidance in preparing adult zebrafish retinal slices, and Eva Ma and Gail Stanton for assistance generating mito-GCaMP and mito-cpYFP transgenic zebrafish.

The authors declare no competing financial interests.

*M.M.G. and W.M.C. contributed equally to this work.

Correspondence should be addressed to Susan E. Brockerhoff, Department of Biochemistry, University of Washington, 750 Republican St., E261, Seattle, WA 98109. E-mail: sbrocker@uw.edu.

DOI:10.1523/JNEUROSCI.2689-16.2017

 0270-6474/17/372061-12$15.00/0

Calcium ions (Ca^{2+}) regulate key pathways in each photoreceptor compartment. At the outer segment, extreme changes in intracellular free Ca^{2+} concentration ($[Ca^{2+}]_i$) mediate phototransduction response recovery that causes a change in membrane potential (Kawamura and Murakami, 1991; Gorczyca et al., 1995; Dizhoor, 2000). In the cell body, Ca^{2+} is stored in mitochondria and endoplasmic reticulum (ER), where it can influence metabolism (Wan et al., 1989; Jouaville et al., 1999; Glancy et al., 2015; Du et al., 2016) and protein trafficking (Beckers and Balch, 1989; Booth and Koch, 1989). At the synapse, Ca^{2+} influx is critical for release of glutamate-containing synaptic vesicles (Rieke and Schwartz, 1996; Thoreson et al., 2004; Heidelberger et al., 2005; Schmitz, 2014). Given the distinct roles of Ca^{2+} in each photoreceptor compartment, tight control of Ca^{2+} domains is crucial for normal cell function.

Mitochondrial Ca^{2+} uptake results in variety of physiological outcomes, including fundamental processes such as protein acetylation in endothelial cells (Marcu et al., 2014). In neurons, mitochondria buffer Ca^{2+} in areas of high axonal firing to produce ATP (MacAskill et al., 2009) and mitigate excitotoxicity via the mitochondrial Ca^{2+} uniporter (MCU) (Qiu et al., 2013; Wang et

al., 2015). In muscle, mitochondrial Ca^{2+} couples metabolic output to contraction (Kwong et al., 2015) and influences muscle size (Mammucari et al., 2015). Past studies have indicated that photoreceptor mitochondria can act as a Ca^{2+} sink, particularly in cones, and it has been suggested that mitochondria may shield the cell body and synapse from potentially harmful high $[Ca^{2+}]_i$ in the outer segment (Szikra and Krizaj, 2007).

Photoreceptor mitochondria are spatially and biochemically poised to regulate cellular Ca^{2+}. Electron microscopy of cones reveals abundant mitochondria within the ellipsoid region of the cell body, just below the outer segment (Tarboush et al., 2012; Masuda et al., 2016). Mitochondria in other tissues are capable of storing large amounts of Ca^{2+} as inorganic phosphate salts (Greenawalt et al., 1964). The MCU is thought to be the primary entry point for Ca^{2+} into the mitochondrial matrix in all cells (De Stefani et al., 2011), although this has not been shown for photoreceptors.

We evaluated the role of mitochondria in maintaining distinct Ca^{2+} domains. We used serial block-face scanning electron microscopy to assemble the 3D morphology of the zebrafish cone ellipsoid. A dense cluster of mitochondria extends to the plasma membrane directly between the outer segment and cell body. We further developed a method to visualize Ca^{2+} dynamics in live retinal slices from adult zebrafish. By manipulating $[Ca^{2+}]_i$ in the presence of a genetically encoded fluorescent Ca^{2+} reporter, we found that cone mitochondria act via the MCU to segregate outer segment and cell body Ca^{2+} pools. This finding suggests a significant role for cone mitochondria in the Ca^{2+} compartmentalization that is required for proper function and regulation of core cellular processes such as phototransduction and metabolism.

Materials and Methods

Zebrafish maintenance. Research was authorized by the University of Washington Institutional Animal Care and Use Committee. Transgenic heterozygotes in the AB or Roy $^{-/-}$ genetic background were maintained in the University of Washington South Lake Union aquatics facility at 27.5°C on a 14 h/10 h light/dark cycle. Fish used for experiments were male and female siblings between 9 and 20 months old.

Generation of transgenic zebrafish. The transgenic lines *Tg(gnat2:GCaMP3)* (Ma et al., 2013; RRID:ZDB-FISH-150901–1755), *Tg(gnat2:ER-GFP)* (George et al., 2014; RRID:ZDB-FISH-150901–7809), and *Tg(gnat2:EGFP)* (Kennedy et al., 2007; RRID:ZDB-FISH-150901-6625) have been described previously. DNA constructs expressing mito-GCaMP3 (Esterberg et al., 2014) or mito-cpYFP (Wang et al., 2008) downstream of the zebrafish cone transducin promoter *gnat2* were generated using the Gateway-Tol2 system (Kwan et al., 2007). These constructs were injected into embryos at the 1- to 2-cell stage with Tol2 transposase mRNA. Mosaic larvae isolated at 5 d after fertilization were raised to adulthood and a germline carrier with a single insertion was identified for each strain, *Tg(gnat2:mito-GCaMP3)* and *Tg(gnat2:mito-cpYFP)*.

Zebrafish retinal slice preparation. Transgenic adult zebrafish were dark adapted >1 h, killed, enucleated, and the retinas immediately dissected away under red light into cold oxygenated Ringer's solution containing the following (in mM): 133 NaCl, 2.5 KCl, 1.5 NaH_2PO_4, 2 $CaCl_2$, 1.5 $MgCl_2$, 10 HEPES, 10 D-glucose, 1 sodium lactate, 0.5 L-glutamine, 0.5 reduced glutathione, 0.5 sodium pyruvate, and 0.3 sodium ascorbate, pH 7.4. Isolated retinas were mounted on filter paper (0.45 μm pore, mixed cellulose; Millipore), flattened with gentle suction, stained 10 min at 20–22°C with dilute BODIPY 558/568 C12 (Invitrogen), and washed with excess Ringer's solution. Flat-mounted retinas were either imaged directly or sliced into 400 μm slices using a tissue slicer (Stoelting). Slices were rotated 90° and the filter paper edges buried in strips of wax on a coverslip for imaging experiments. To assay cell viability, retinal slices without BODIPY were stained with 7.5 μM propidium iodide (PI) (Invitrogen) 20 min at 20–22°C and washed 3 times before imaging.

Ca^{2+} imaging. Retinal slices were imaged in either static Ringer's solution or in a flow chamber attached to an injection apparatus and perfusion system flowing freshly oxygenated Ringer's solution at 20–22°C. Experiments involving Ca^{2+}-free conditions were conducted with a modified Ringer's solution containing 0.4 μM EGTA instead of $CaCl_2$, pH 7.4. Experiments involving Na^+-free conditions were conducted using another modified isotonic Ringer's solution containing the following (in mM): 147 Tris, ~120 HCl, 1 KCl, 2 $CaCl_2$, 1.5 $MgCl_2$, 1.5 KH_2PO_4, 10 HEPES, 10 D-glucose, 0.5 L-glutamine, and 0.5 reduced glutathione, pH 7.4. Flat mounts and slices were imaged on either an Olympus FV1000 or a Leica LSP8 confocal microscope with a 40× water objective; excitation/emission wavelengths were 488/510 nm for fluorescent proteins and 559/594 nm for BODIPY and PI. Olympus FluoView (RRID:SCR_014215) or Leica LAS-X (RRID:SCR_013673) software was used to acquire images and time-lapse images were taken every 10 s. For quantification of absolute mito-GCaMP fluorescence, *z*-stacks of retinal sections were generated from 10–20 1 μm slices.

Pharmacological treatments. Ca^{2+} modulators were injected into the perfusion chamber after 2 min of baseline time-lapse imaging, followed by a single pump of the syringe to aid mixing. For KCl depolarization experiments, a concentrated solution of KCl in Ringer's solution was injected into perfusion chamber to reach a final concentration of 10 mM. Sildenafil citrate (Sigma-Aldrich) was stored in DMSO at 20 mM and used at a working concentration of 25 μM. Thapsigargin (Sigma-Aldrich) was stored in DMSO at 10 mM and used at a working concentration of 1 μM. 50 mM KB-R7943 mesylate (Tocris Bioscience) was prepared fresh each day in DMSO and used at final concentration of 100 μM. Ru360 (Millipore) was prepared fresh for each experiment, first dissolved in cold deoxygenated water to 5 mM, and then stored on ice for <3 h; immediately before incubation, it was diluted in Ringer's solution to 10 μM. Where indicated, retinal slices were incubated 1 h in 10 μM Ru360 at 20–22°C before imaging and maintained in 10 μM Ru360 throughout the duration of experiments.

Electron microscopy. Adult zebrafish eyes were enucleated, the anterior half was dissected away, and the eyecup was cut in half. Tissue was fixed in 4% glutaraldehyde in 0.1 M sodium cacodylate buffer, pH 7.2, at room temperature (RT), then stored overnight at 4°C. Samples were washed 4 times in sodium cacodylate buffer, postfixed in osmium ferrocyanide (2% osmium tetroxide/3% potassium ferrocyanide in buffer) for 1 h on ice, washed, incubated in 1% thiocarbohydrazide for 20 min, and washed again. After incubation in 2% osmium tetroxide for 30 min at RT, samples were washed and *en bloc* stained with 1% aqueous uranyl acetate overnight at 4°C. Samples were finally washed and *en bloc* stained with Walton's lead aspartate for 30 min at 60°C, dehydrated in a graded ethanol series, and embedded in Durcupan resin. Serial sections were cut at 60 nm thickness and imaged with 6 nm pixel size using a Zeiss Sigma VP scanning electron microscope fitted with a Gatan 3View2XP ultramicrotome apparatus. Imaged stacks were concatenated and aligned using TrakEM2 (RRID:SCR_008954). Unless stated otherwise, five washes with water were used for all wash steps.

Image processing and analysis. Time-lapse images were analyzed using ImageJ software (RRID:SCR_002285). Time lapses were corrected for *X–Y* drift using the MultiStackReg plugin and regions of interest (ROIs) selected around individual cell compartments. Separate red and green kymographs were generated as described previously (Ma et al., 2013) from ROIs for the synapse, cell body, and outer segment or ellipsoid regions and were used to quantify fluorescence changes in single cells. Data were compiled using Microsoft Excel. To account for focal plane variance and drift in the *z*-direction, the green GCaMP fluorescence signal was divided by the red BODIPY fluorescence signal at each time point. Fold change was calculated from $t = 0$ using the equation $F/F_0 = (510_t/594_t)/(510_0/594_0)$. For *z*-stacks, absolute mito-GCaMP fluorescence was measured from frames at the widest part of individual mitochondrial clusters. Brightness and contrast were adjusted equally in the presented images to ease visualization.

Statistics. Results are reported as mean ± SEM. R (RRID:SCR_001905) with R Commander (Fox, 2005) was used to perform one-way ANOVA

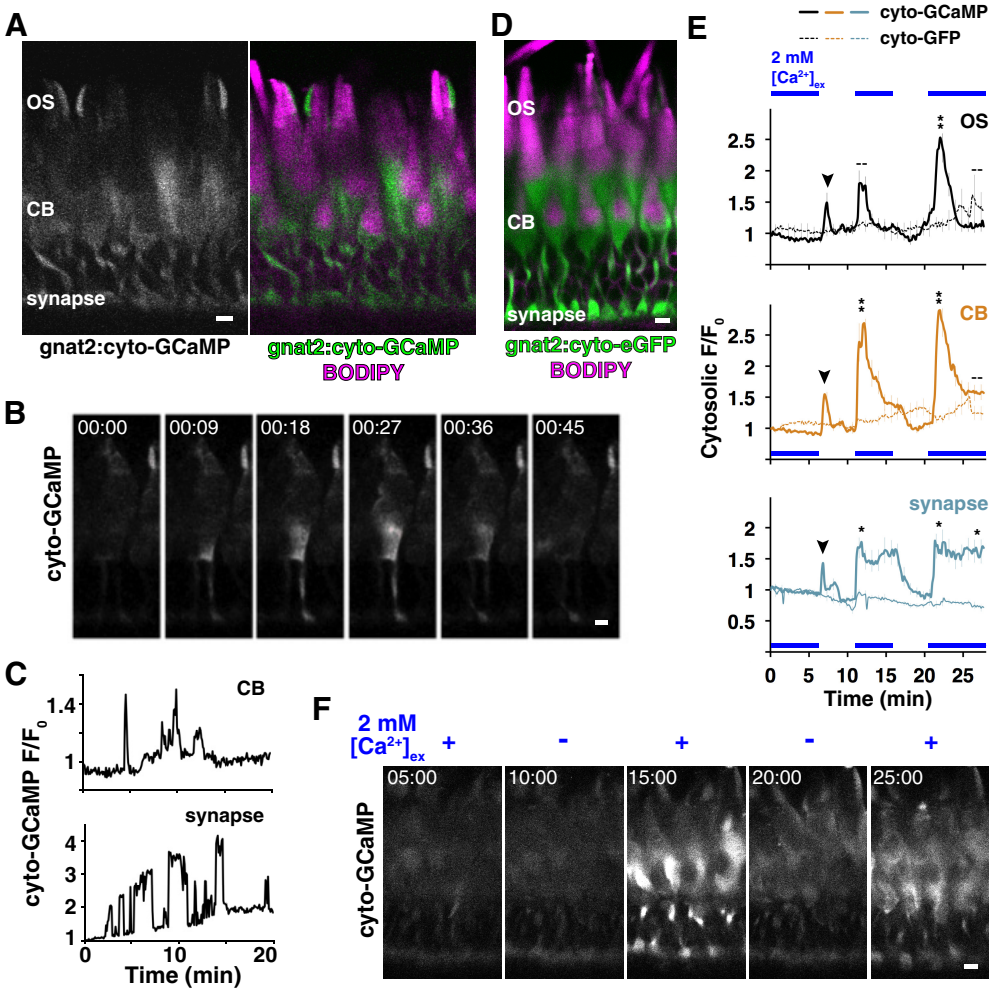

Figure 1. Cone photoreceptors undergo transient Ca^{2+} flashes and are sensitive to extracellular Ca^{2+} flux. ***A***, Representative confocal image of *in situ* retinal slice from transgenic dark-adapted zebrafish expressing cyto-GCaMP in cones (left) and overlaid with BODIPY membrane stain (right). Areas of bright cyto-GCaMP fluorescence in the outer segment layer appear to be the zebrafish accessory outer segment. ***B***, Montage of confocal images depicting spontaneous cyto-GCaMP Ca^{2+} flash in a single cone. ***C***, Graphs showing discrete and spontaneous Ca^{2+} flashes in the synapse and cell body of a single cone over 20 min. ***D***, Representative confocal image of retinal slice from transgenic dark-adapted zebrafish expressing cyto-GFP in cone PRs (green) stained with BODIPY membrane stain (magenta). ***E***, Mean fluorescence responses of cone compartments during consecutive washouts of extracellular Ca^{2+} with buffer containing 0.4 μM EGTA. Solid lines, cyto-GCaMP (3 experiments; *n* for OS = 27, CB = 31, synapse = 40); dashed lines, cyto-GFP control (1 experiment; *n* for OS = 15, CB = 15, synapse = 18); blue bars, presence of 2 mM extracellular Ca^{2+}. Arrowheads indicate transient burst of Ca^{2+} in all compartments after initial Ca^{2+} washout. One-way ANOVA was performed at 12:00, 22:00, and 27:00 for cyto-GCaMP versus cyto-GFP; $*p < 0.05$; $**p < 0.001$; –, not significant. ***F***, Montage of confocal images depicting cyto-GCaMP responses to Ca^{2+} washout quantified in ***E***. Error bars indicate SEM; *n* represents number of single cells analyzed. Scale bars, 5 μm; timescale = min:sec. OS, Outer segment; CB, cell body.

for multiple comparisons or two-tailed *t* tests with a 99% confidence interval for pairwise comparisons.

Results

Genetically encoded Ca^{2+} reporter senses cytosolic $[Ca^{2+}]$ in zebrafish cones.

Larval zebrafish cones display cytosolic Ca^{2+} transients heterogeneous in magnitude and duration (Ma et al., 2013). To understand normal Ca^{2+} dynamics in adult zebrafish cones, we analyzed $[Ca^{2+}]_i$ changes using fresh retinal slices from adult zebrafish stably expressing the genetically encoded Ca^{2+} sensor GCaMP3 in cone photoreceptor cytosol (cyto-GCaMP) (Fig. 1*A*). Photoreceptors in retinal slices do not take up the stain PI for at least 4 h, indicating that the cells remain viable (data not shown). Confocal time-lapse imaging of slices revealed that adult cones undergo Ca^{2+} transients in the synapse and cell body similar to larval cones (Fig. 1*B*,*C*).

To determine whether $[Ca^{2+}]_i$ is sensitive to extracellular Ca^{2+} concentration ($[Ca^{2+}]_{ex}$), we time-lapse imaged cyto-GCaMP retinal slices while using perfusion to exchange the surrounding 2 mM Ca^{2+} Ringer's solution with Ca^{2+}-free solution containing 0.4 μM EGTA (Fig. 1*E*,*F*). Initial removal of extracellular Ca^{2+} transiently, but robustly, increased cyto-GCaMP fluorescence, indicating possible Ca^{2+} release from internal stores (Fig. 1*E*, arrowheads). When $[Ca^{2+}]_{ex}$ was returned to 2 mM, Ca^{2+} influx into the synapse and cell body increased cyto-GCaMP fluorescence 1.5 ± 0.2-fold and 2.7 ± 0.3-fold, respectively (15 min time point; Fig. 1*E*,*F*). A second washout and return to 2 mM Ca^{2+} raised $[Ca^{2+}]_i$ in all compartments (at 22 min, outer segment, 2.5 ± 0.3-fold; cell body, 2.9 ± 0.3-fold; synapse, 1.6 ± 0.2-fold). Further, each cell compartment responded with unique kinetics and amplitude, indicating that Ca^{2+} in cones is not one continuous pool. To confirm that changes in cyto-GCaMP fluorescence report $[Ca^{2+}]_i$, we showed that fluorescence of cones expressing cytosolic eGFP (cyto-GFP; Fig. 1*D*) (Kennedy et al., 2007) is not sensitive to fluctuations in $[Ca^{2+}]_{ex}$ (Fig. 1*E*, dashed lines).

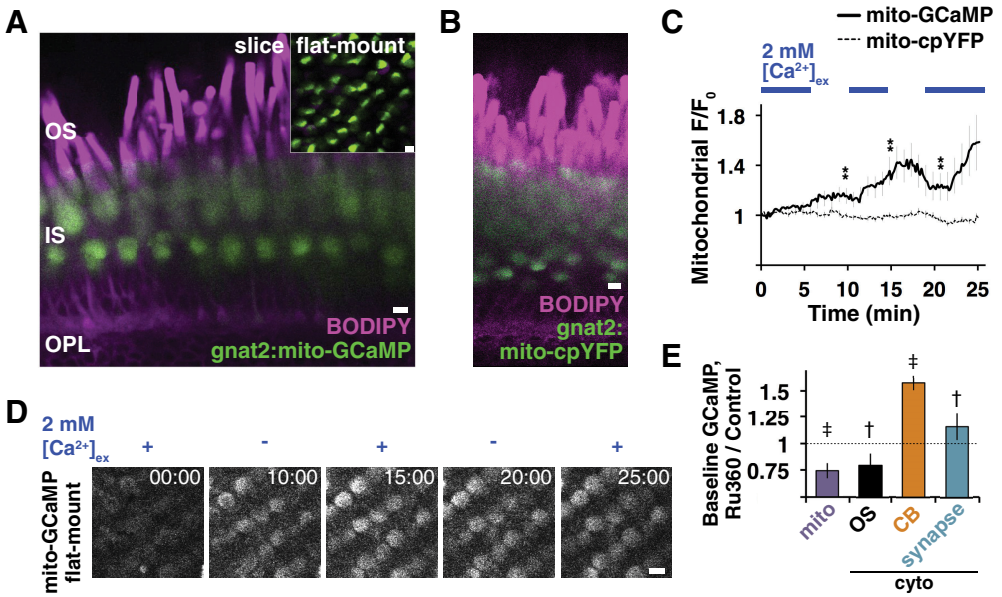

Figure 2. Cone mitochondria buffer intracellular Ca^{2+}. ***A***, Representative confocal images of *in situ* slice or flat-mount (inset) from transgenic dark-adapted zebrafish expressing mito-GCaMP in cone PRs (green) and stained with BODIPY membrane stain (magenta). ***B***, Representative confocal image of retinal slice from transgenic dark-adapted zebrafish expressing mito-cpYFP in cone PRs (green) stained with BODIPY membrane stain (magenta). ***C***, Mean fluorescence responses of cone mitochondria during consecutive washouts of extracellular Ca^{2+} with buffer containing 0.4 μM EGTA. Solid lines, mito-GCaMP (4 experiments; $n = 45$ cells); dashed lines, mito-cpYFP control (4 experiments; $n = 56$ cells); blue bars, presence of 2 mM extracellular Ca^{2+}. One-way ANOVA was performed at 10:00, 15:00, and 22:00 for mito-GCaMP versus mito-cpYFP; $^{**}p < 0.001$. ***D***, Montage of flat-mount confocal images depicting mito-GCaMP Ca^{2+} responses quantified in ***C***. ***E***, Bar graph depicting mean baseline mito-GCaMP and cyto-GCaMP fluorescence changes resulting from Ru360 preincubation (n for mitochondria = 15 experiments, 143 cells per condition; for OS = 3 experiments, 39 cells per condition; for CB = 3 experiments, 25 cells per condition; for synapse = 3 experiments, 24 cells per condition). Two-tailed t tests were performed for each compartment for GCaMP control versus GCaMP Ru360; †$p < 0.05$, ‡$p < 0.001$. Error bars indicate SEM. Scale bars, 5 μm; timescale = min:sec. OS, Outer segment; IS, inner segment; OPL, outer plexiform layer; CB, cell body.

$[Ca^{2+}]$ in the mitochondrial matrix is influenced by cytosolic $[Ca^{2+}]$.

Mitochondria can buffer Ca^{2+}, an activity vital to homeostasis in neurons (Qiu et al., 2013; Esterberg et al., 2014). To monitor free Ca^{2+} concentration within the mitochondrial matrix ($[Ca^{2+}]_m$) of cones, we used transgenic zebrafish that stably express GCaMP3 targeted to the matrix of cone mitochondria (mito-GCaMP; Fig. 2*A*). Under basal time-lapse imaging conditions, mito-GCaMP retinal slices and flat mounts displayed no fluctuation of fluorescence (data not shown) and mitochondria remained clustered at the base of the outer segment. Alternating $[Ca^{2+}]_{ex}$ from 2 to 0 mM induced modest but significant changes in $[Ca^{2+}]_m$ throughout the entire cluster (Fig. 2*C*,*D*). Given that identical conditions elicit large changes in cyto-GCaMP, these data suggest that mitochondria can take up free cytosolic Ca^{2+}, although mito-GCaMP responses were generally slower. In contrast, zebrafish retinas expressing circularly permuted YFP in cone mitochondria (mito-cpYFP; Fig. 2*B*), which is not directly sensitive to Ca^{2+} (Wang et al., 2008), did not respond to altering $[Ca^{2+}]_{ex}$ (Fig. 2*C*, dashed lines).

In other cells, Ca^{2+} flows into mitochondria through the MCU (Williams et al., 2013), so we investigated whether the MCU is responsible for mitochondrial Ca^{2+} uptake in cones. We imaged 3D stacks of mito-GCaMP retinal slices incubated for 1 h in either Ringer's solution or 10 μM Ru360, a specific inhibitor of the MCU (Matlib et al., 1998; Kirichok et al., 2004; Baughman et al., 2011). Mito-GCaMP fluorescence of individual cells was measured at the center of the mitochondrial cluster (Fig. 2*E*). Ru360 treatment decreased absolute GCaMP fluorescence of mitochondrial clusters by 25.4 ± 7.1% (Fig. 2*E*). Similar to other cells, Ca^{2+} uptake into cone mitochondria appears to occur through the MCU. One hour of Ru360 incubation also altered baseline fluorescence of cyto-GCaMP retinal slices, decreasing outer segment signal 20.1 ± 11.0% and increasing cell body and synaptic fluorescence 56.9 ± 6.9% and 16.2 ± 12.5%, respectively (Fig. 2*E*). This suggests that Ca^{2+} homeostasis throughout the cell is influenced by mitochondrial Ca^{2+} uptake.

Cone ellipsoid contains a tight cluster of mitochondria.

In photoreceptors, the unique morphology and localization of mitochondria (Tarboush et al., 2012, 2014) suggest that they can influence Ca^{2+} homeostasis even more than in other cells. To understand the 3D arrangement of mitochondria within the ellipsoid region of cones, we performed serial block-face scanning electron microscopy of adult zebrafish retina (Fig. 3*A*). Mitochondria in zebrafish cones form a tight cluster in the ellipsoid just below the connecting cilium and outer segment. The mitochondrial cluster is comprised of ~80 individual mitochondria densely packed together with the outer membranes of individual mitochondria directly adjacent to one another (Fig. 3*B*). A 3D reconstruction shows that the cluster occupies the majority of the cell volume between the outer segment and cell body (Fig. 3*C*). The abundance and very tight juxtaposition of the mitochondria supports the hypothesis that the mitochondrial cluster in zebrafish cones can act as a barrier to diffusion between the outer segment and cell body.

Contacts between ER and mitochondria facilitate mitochondrial Ca^{2+} uptake in many cell types (Rowland and Voeltz, 2012). ER in photoreceptors is confined to the synapse and cell body (Mercurio and Holtzman, 1982) and we evaluated the extent of interactions between ER and mitochondria in the cell body. Using adult zebrafish from a transgenic line expressing GFP targeted to cone ER (ER-GFP) (George et al., 2014), we found that the ER forms a basket-like network under the mitochondrial cluster, but

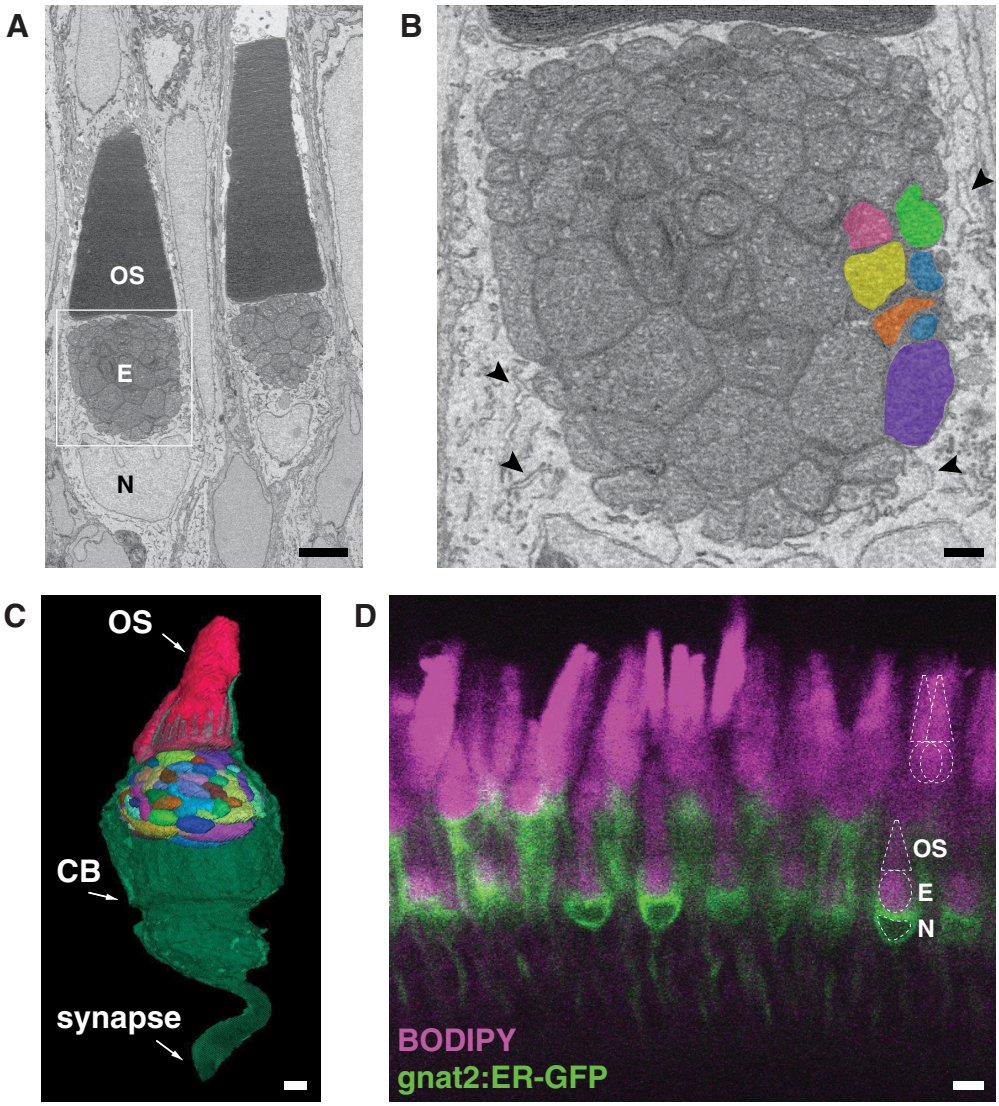

Figure 3. Cone mitochondria densely pack the interface between the inner and outer segments. ***A***, Scanning electron microscopy image of two zebrafish cones showing dense packing of the mitochondrial cluster. ***B***, Magnification of boxed region in ***A*** showing the center of the mitochondrial cluster. The ER is indicated with arrowheads; matrices of six individual mitochondria are colored. ***C***, 3D reconstruction from serial block-face scanning electron microscopy of an adult zebrafish cone; individual mitochondria are uniquely colored and outer segment is colored red. The tip of the outer segment and cone pedicle were not rendered in this image. ***D***, Representative confocal image of *in situ* transgenic zebrafish retinal slice expressing ER-targeted GFP in cones (green) and stained with BODIPY membrane stain (magenta). Scale bars: ***A***, 10 μm; ***B***, 2 μm; ***C***, 1 μm; ***D***, 5 μm. E, Ellipsoid; N, nucleus; OS, outer segment; CB, cell body.

does not appear to enter into the tight cluster of mitochondria (Fig. 3*D*). Furthermore, in scanning electron microscopy images used for 3D reconstruction, we did not find evidence of ER within the mitochondria cluster nor between the outer segment and apical face of the mitochondrial cluster (Fig. 3*B*).

Ca^{2+} confinement to the inner segment is mediated by mitochondria

To evaluate Ca^{2+} compartmentalization, we used two strategies to increase inner segment $[Ca^{2+}]_I$ specifically. We depolarized cones by perfusing retinal sections with Ringer's solution containing elevated [KCl] while time-lapse imaging (Fig. 4*A*, top). Depolarization of the plasma membrane activates L-type voltage gated Ca^{2+} channels at the synapse and cell body (Taylor and Morgans, 1998; Kourennyi and Barnes, 2000; Lee et al., 2015), allowing Ca^{2+} to flow into those compartments. We found that increasing extracellular [KCl] from 2.5 to 10 mM evoked a >2-fold rise in cyto-GCaMP fluorescence in the synapse and cell body but, notably, no increase in fluorescence in the outer segment (Fig. 4*B*, light solid lines). A modest 13 ± 3% increase in mito-GCaMP fluorescence persisted 5 min after increasing extracellular [KCl] (Table 1), suggesting that mitochondria are capable of Ca^{2+} uptake from the cell body pool, perhaps via the ER. Cyto-GFP (Fig. 4*B*, dashed lines) and mito-cpYFP (Table 1) retinal slices were insensitive to KCl.

We hypothesized that reducing Ca^{2+} uptake into cone mitochondria could attenuate Ca^{2+} compartmentalization and lead to increases in outer segment $[Ca^{2+}]_i$, so we preincubated cyto-GCaMP retinal slices in Ru360, then depolarized them with 10 mM KCl (Fig. 4*A*, bottom arrowheads). Outer segment fluorescence increased transiently 1.80 ± 0.04-fold compared with untreated slices (Fig. 4*B*, dark solid lines), but synapse $[Ca^{2+}]_i$ was unaffected by Ru360. This is consistent with the absence of mitochondria at the zebrafish cone synaptic terminal (Fig. 2*A*), unlike in other teleost ribbon synapses (Zenisek and Matthews, 2000). Ten minutes after KCl depolarization, Ru360 treatment

decreased cell body fluorescence slightly (1.41 ± 0.09-fold vs 1.18 ± 0.03-fold, $p = 0.045$), perhaps indicative of enhanced cell body Ca^{2+} extrusion through now-accessible rapid Na^+/K^+-Ca^{2+} exchangers on the outer segment. Redistribution of Ca^{2+} into the outer segment after Ru360 treatment suggests that compartmentalization requires efficient uptake of Ca^{2+} by mitochondria through the MCU.

Given the distinct localization of cone ER in the cell body and synapse (George et al., 2014), we hypothesized that blocking ER Ca^{2+} uptake would increase cytosolic $[Ca^{2+}]_i$ in those compartments. Whereas time-lapse imaging, cyto-GCaMP retinal slices were treated with thapsigargin, a sarco-endoplasmic reticulum Ca^{2+} ATPase (SERCA) inhibitor that blocks pumping of Ca^{2+} into the ER (Fig. 4*C*, top) (Lytton et al., 1991). Thapsigargin caused rapid and sustained apparent $[Ca^{2+}]_i$ increase in the synapse, where ER regulates Ca^{2+} levels that mediate synaptic vesicle release (Chen et al., 2015) and in the cell body (Fig. 4*D*, light solid lines). Thapsigargin also increased mito-GCaMP fluorescence 14 ± 7% 5 min after treatment (Table 1). However, there was no change in outer segment cyto-GCaMP fluorescence, indicating that, consistent with ER localization presented in Figure 3*D*, ER does not directly affect outer segment $[Ca^{2+}]_i$.

We again wondered whether mitochondrial Ca^{2+} uptake was insulating the outer segment from cell body $[Ca^{2+}]_i$ fluctuations. When mitochondrial Ca^{2+} uptake is reduced with Ru360, we detected modest but steady apparent increases in outer segment $[Ca^{2+}]_i$ after thapsigargin treatment (Figs. 4*C*, bottom arrowheads, 4*D*, dark solid lines). Thapsigargin did not elicit fluorescence changes in our control indicators, cyto-GFP (Fig. 4*D*, dashed lines) and mito-cpYFP (Table 1). Together, these results suggest that MCU enables mitochondria to sequester cell body Ca^{2+} and prevent its flow to the outer segment.

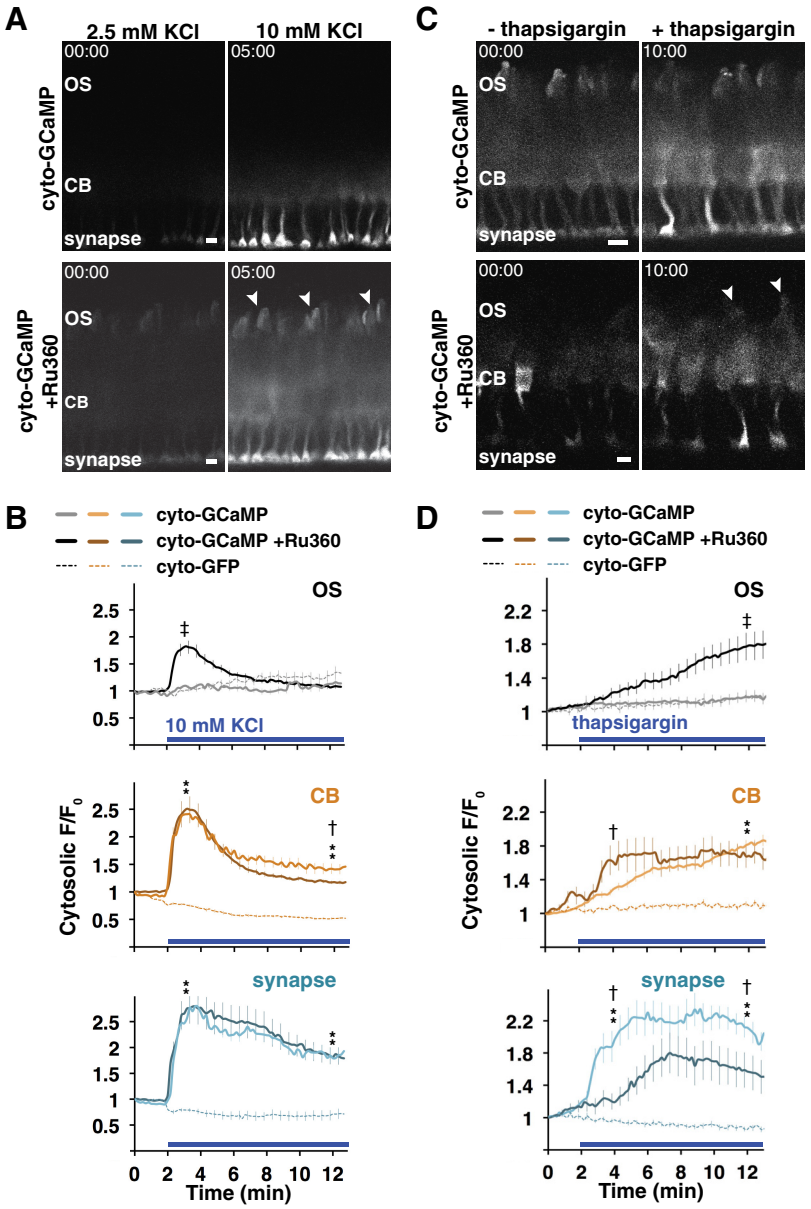

Figure 4. Cytosolic Ca^{2+} from the inner segment is isolated from the outer segment. ***A***, Representative confocal image of *in situ* retinal slices from transgenic dark-adapted zebrafish expressing cyto-GCaMP in cones before and after increasing extracellular [KCl] from 2.5 to 10 mM. Top, Control. Bottom, 1 h preincubation with 10 μM Ru360. Arrowheads indicate single outer segments containing redistributed Ca^{2+}. ***B***, Mean fluorescence responses of single cone outer segment (OS) (top), cell body (CB) (middle), and synapses (bottom) during KCl depolarization. Light solid lines, cyto-GCaMP control (4 experiments; *n* for OS = 47, CB = 44, synapses = 53); dark solid lines, cyto-GCaMP with Ru360 preincubation (3 experiments; *n* for OS = 43, CB = 36, synapses = 34); dashed lines, cyto-GFP control (2 experiments; *n* for OS = 20, CB = 20, synapses = 20); blue bars, presence of 10 mM extracellular KCl. ***C***, Representative confocal image of cyto-GCaMP-expressing retinal slices before and after treatment with 1 μM thapsigargin, an inhibitor of ER Ca^{2+} uptake. Top, Control. Bottom, Ru360 preincubation. Arrowheads indicate single outer segments containing redistributed Ca^{2+}. ***D***, Mean fluorescence responses of single cone OS (top), CB (middle), and synapses (bottom) during thapsigargin treatment. Light solid lines, cyto-GCaMP control (3 experiments; *n* for OS = 29, CB = 27, synapses = 30); dark solid lines, cyto-GCaMP with Ru360 preincubation (3 experiments; *n* for OS = 29, CB = 37, synapses = 33); dashed lines, cyto-GFP control (2 experiments; *n* for OS = 20, CB = 20, synapses = 20); blue bars, presence of 1 μM thapsigargin. One-way ANOVA was performed at 03:00 and 12:00 for cyto-GCaMP versus cyto-GFP (**$p < 0.001$) and cyto-GCaMP control versus cyto-GCaMP Ru360 (†$p < 0.05$, ‡$p < 0.001$). Error bars indicate SEM; *n* represents number of single cells analyzed. Scale bars, 5 μm; timescale = min:sec.

Na^+/K^+-Ca^{2+} exchanger activity maintains low outer segment $[Ca^{2+}]_i$

At the cone plasma membrane, ion exchangers release intracellular Ca^{2+} and bring in extracellular Na^+. The Na^+/K^+-Ca^{2+} exchanger NCKX has high activity and is localized exclusively at the outer segment to support rapid Ca^{2+} clearance during phototransduction. A lower-affinity Na^+-Ca^{2+} exchanger, NCX1, localizes to cone inner segments, but most Ca^{2+} extrusion from the inner segment and synapse happens through plasma membrane Ca^{2+}-ATPases (PMCA) confined to those compartments (Krizaj and Copenhagen, 1998; Johnson et al., 2007). We investigated whether mitochondrial Ca^{2+} buffering plays a role in the functional disparity of extrusion mechanisms, contributing to Ca^{2+} compartmentalization in cones, and used two strategies to address this.

First, we inhibited Ca^{2+} efflux through the plasma membrane exchangers by using perfusion to bathe GCaMP retinal slices in

Table 1. Mitochondrial fluorescence changes of retinal slices after 5 min treatment with Ca^{2+} modulators

Condition	Mito-cpYFP[a]	Mito-GCaMP	*p*-value[b]
KCl	0.86 ± 0.02 (*n* = 61)	1.13 ± 0.03 (*n* = 28)	0.005
Thapsigargin	0.86 ± 0.03 (*n* = 31)	1.14 ± 0.07 (*n* = 65)	0.038
Na^+ depletion	1.64 ± 0.06 (*n* = 21)	1.40 ± 0.04 (*n* = 72)	—
KB-R7943	0.74 ± 0.04 (*n* = 20)	1.07 ± 0.03 (*n* = 42)	0.002
Sildenafil	0.86 ± 0.08 (*n* = 37)	1.10 ± 0.05 (*n* = 60)	0.072
KB-R7943[c] + sildenafil	—	1.38 ± 0.06 (*n* = 72)	0.0002
KB-R7943[c] + Ru360[c] + sildenafil	—	1.09 ± 0.05 (*n* = 30)	0.003
DMSO	—	0.89 ± 0.04 (*n* = 9)	—

[a]*n* = number of single mitochondrial clusters. Values are shown as F/F_0 ± SEM.

[b]Paired *t* test for mito-GCaMP treatment versus DMSO, two-tailed, 99% confidence interval.

[c]Preincubation.

Ringer's solution devoid of Na^+ (Schnetkamp et al., 1991) while time-lapse imaging (Fig. 5*A*). Isotonic depletion of Na^+ from the bath caused robust and very rapid increases in cyto-GCaMP fluorescence that initiated at the outer segment and propagated gradually into the cell body, with only a modest and very slow increase in the synapse (Fig. 5*B*, solid lines). These findings indicate that outer segment $[Ca^{2+}]_i$ can be maintained at high levels independently of inner segment $[Ca^{2+}]_i$. Na^+ depletion also increased fluorescence of both mito-GCaMP and mito-cpYFP retinal slices (Table 1), indicative of changes in mitochondrial membrane potential.

Second, we treated cyto-GCaMP retinal slices with an inhibitor of Na^+/Ca^{2+} exchangers, KB-R7943 (Iwamoto et al., 1996; Vinberg et al., 2015) while time-lapse imaging (Fig. 5*C*). Similar to Na^+ depletion, blocking Ca^{2+} extrusion from the exchangers elicited a rapid and sustained increase in outer segment cyto-GCaMP fluorescence, followed by a slower increase in the cell body and only a small, transient response at the synapse (Fig. 5*D*, solid lines). Consistent with reports of KB-R7943 promoting mitochondrial Ca^{2+} retention (Wiczer et al., 2014), mito-GCaMP fluorescence rose 7 ± 3% after 5 min in KB-R7943, a small but significant increase compared with DMSO alone (Table 1). Cyto-GFP retinal slices were unaffected by Na^+ depletion and KB-R7943 (Fig. 5*B*,*D*, dashed lines). Together, these results suggest that extrusion is compartmentalized and demonstrate that flow of cytosolic Ca^{2+} between the outer segment and the cell body is regulated.

Cone mitochondria buffer Ca^{2+} from the outer segment.

To establish whether mitochondria buffer outer segment Ca^{2+}, we used sildenafil, an inhibitor of the phosphodiesterase PDE6 (Zhang et al., 2005), to increase outer segment $[Ca^{2+}]_i$ selectively. PDE6 inhibition causes cGMP to build up in the outer segment, opening more cGMP-gated channels and allowing outer segment Ca^{2+} accumulate. Accordingly, treating cyto-GCaMP retina slices with sildenafil brought on a sustained increase in outer segment fluorescence (Fig. 6*A*, top). The addition of sildenafil also causes transient increases in both cell body and synapse $[Ca^{2+}]_i$ because influx of cations into the outer segment depolarizes the cell (Fig. 6*B*, solid lines). This Ca^{2+} burst diminishes in the cell body and synapse within 5 min, but outer segment $[Ca^{2+}]_i$ remains elevated ~2-fold. Sildenafil had no effect on the fluorescence of cyto-GFP retinal slices (Fig. 6*B*, dashed lines).

When mito-GCaMP or mito-cpYFP retinal slices were treated with sildenafil, we noticed an apparent elongation of mitochondrial clusters (Fig. 6*A*, bottom), similar to morphological changes brought on by retinomotor movements in prolonged darkness (Burnside et al., 1993). Mito-GCaMP fluorescence of a region at the center of the cluster increased slightly (Fig. 6*F*, light solid line), but this change was not significant compared with the vehicle DMSO alone ($p = 0.07$; Table 1). Mito-cpYFP fluorescence was insensitive to sildenafil.

To address the possibility of elevated outer segment $[Ca^{2+}]_i$ simply being extruded via NCKX, we performed two-step perfusion experiments. While time-lapse imaging, we first treated retinal slices with the Na^+/Ca^{2+} exchanger inhibitor KB-R7943, allowed $[Ca^{2+}]_i$ to stabilize for 5 min, and then applied sildenafil (Fig. 6*C*, top row). Subsequent application of sildenafil resulted in larger overall fold changes in cyto-GCaMP fluorescence for all compartments (Fig. 6*D*, dashed lines) and a sustained increase in the cell body consistent with inhibition of Ca^{2+} extrusion.

In a similar experiment, mito-GCaMP retinal slices were pretreated with KB-R7943 for 10 min and then treated with sildenafil (Fig. 6*E*, top). This caused a dramatic increase in mito-GCaMP fluorescence (Fig. 6*F*, dashed line), suggesting that cone mitochondria can accumulate Ca^{2+} when outer segment $[Ca^{2+}]_i$ is very high. To determine whether this Ca^{2+} uptake is mediated by MCU, we repeated this experiment using retinal slices first preincubated in Ru360 (Fig. 6*E*, bottom). One hour of Ru360 preincubation followed by 10 min of additional KB-R7943 preincubation abolished mitochondrial Ca^{2+} uptake (Fig. 6*F*, solid dark line), suggesting that this pool of Ca^{2+} enters mitochondria via the MCU.

Finally, we investigated how MCU activity was mediating cytosolic Ca^{2+} pools. Using cyto-GCaMP retinal slices preincubated in Ru360, we again performed two-step perfusion experiments with KB-R7943 and sildenafil (Fig. 6*C*, bottom row). With both mitochondrial Ca^{2+} uptake and plasma membrane Ca^{2+} extrusion blocked, cyto-GCaMP fluorescence depicted rapid and large increases of $[Ca^{2+}]_i$ in all compartments of the cell (Fig. 6*D*, solid lines). Despite their magnitude, these large Ca^{2+} bursts were cleared from the cytosol of all compartments, including the outer segment, within minutes. Considering that similar conditions elicit no increase in mito-GCaMP fluorescence (Fig. 6*F*, solid dark line) when Na^+/Ca^{2+} exchange is inhibited and $[Ca^{2+}]_i$ is very high, activation of PMCA could provide an exit route for cytosolic Ca^{2+}. Although PMCA localizes at the inner segment and synapse (Krizaj et al., 2002), absent MCU activity outer segment Ca^{2+} appears to redistribute throughout the cell.

These data suggest that mitochondrial Ca^{2+} buffering can insulate the inner segment from a high $[Ca^{2+}]_i$ pool in the outer segment. Under extreme conditions $[Ca^{2+}]_i$ may become high enough to activate MCU in cones and the ER may facilitate Ca^{2+} uptake into a subset of mitochondria. Altogether, our findings show that mitochondria can take up Ca^{2+} from both the outer segment and cell body, effectively separating the two compartments from each other.

Discussion

Compartmentalization of Ca^{2+} has functional implications (Augustine et al., 2003; Yang et al., 2016). In photoreceptors, Ca^{2+} has distinct roles and concentrations in different parts of the cell (Krizaj and Copenhagen, 1998; Sampath et al., 1999). Ca^{2+} influences phototransduction in the outer segment, where $[Ca^{2+}]_i$ ranges from 20–50 nM in light to 300–500 nM in darkness (Krizaj and Copenhagen, 2002). In the adjacent cell body, $[Ca^{2+}]_i$ is in the tens of nanomolar range (Krizaj and Copenhagen, 1998) and Ca^{2+} regulates vital cellular processes such as metabolism (Wan et al., 1989; Satrústegui et al., 2007; Glancy and Balaban, 2012; Du

et al., 2013; Llorente-Folch et al., 2013). How Ca^{2+} concentrations under different physiological conditions are maintained in functionally distinct compartments in polarized neurons, such as photoreceptors, is not understood.

Here, we report direct experimental evidence that mitochondria can create functionally and spatially restricted domains of Ca^{2+} in photoreceptors. Using serial block-face scanning electron microscopy and confocal microscopy we establish that within the ellipsoid region of zebrafish cones, a large and tight cluster of many individual mitochondria forms a diffusion barrier between the cell body and outer segment. The cluster is partially surrounded but not permeated by the ER, known to facilitate Ca^{2+} transfer into mitochondria. We show that mitochondria take up Ca^{2+} in response to changes in $[Ca^{2+}]_i$ in both the cell body and outer segment. Preventing Ca^{2+} uptake by blocking MCU function disrupts the formation of distinct cellular Ca^{2+} domains.

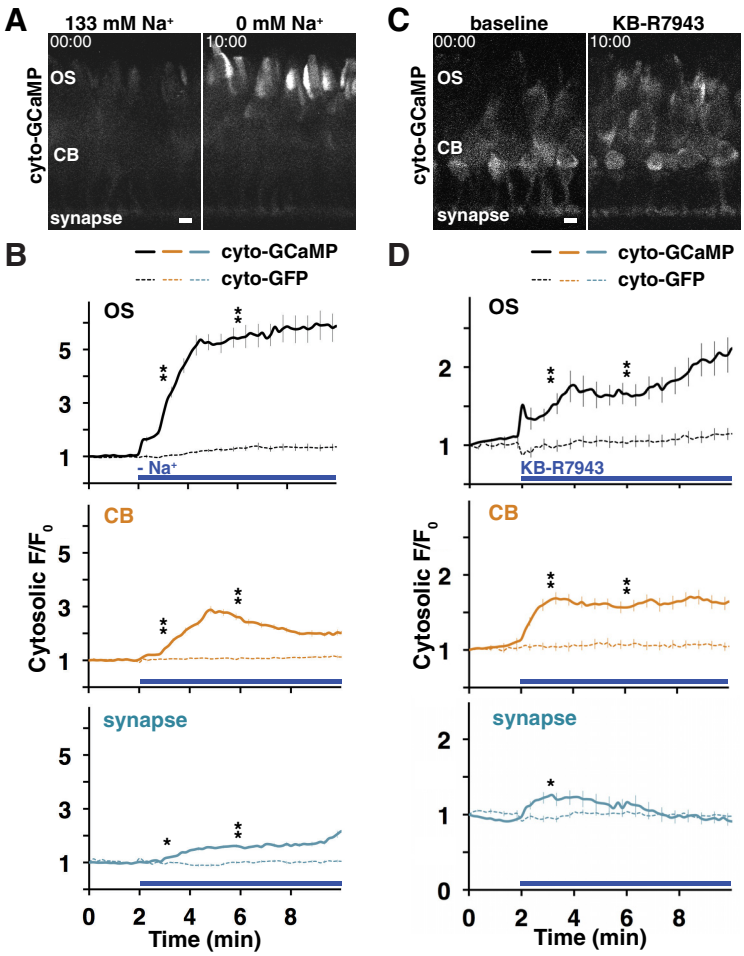

Figure 5. Plasma membrane ion exchange can mediate $[Ca^{2+}]_i$ in the cell body and outer segment. ***A***, Representative confocal image of *in situ* retinal slice from transgenic dark-adapted zebrafish expressing cyto-GCaMP in cones before (left) and after (right) depletion of extracellular Na^+ to halt Ca^{2+} extrusion via Na^+/Ca^{2+} exchangers. ***B***, Mean fluorescence responses of cone outer segment (OS) (top), cell body (CB) (middle), and synapses (bottom) during extracellular Na^+ depletion. Solid lines, cyto-GCaMP (3 experiments; *n* for OS = 77, CB = 68, synapses = 77); dashed lines, cyto-GFP control (2 experiments; *n* for OS = 52, CB = 39, synapses = 47); blue bars, presence of isotonic Na^+-free Ringer's solution. ***C***, Representative confocal image of cyto-GCaMP-expressing retinal slice before (left) and after (right) treatment with 100 μM KB-R7943, an inhibitor of plasma membrane Na^+/Ca^{2+} exchangers. ***D***, Mean fluorescence responses of cone OS (top), CB (middle), and synapses (bottom) during KB-R7943 treatment. Solid lines, cyto-GCaMP (3 experiments; *n* for OS = 19, CB = 30, synapses = 30); dashed lines, cyto-GFP control (3 experiments; *n* for OS = 30, CB = 30, synapses = 30); blue bars, presence of 100 μM KB-R7943. One-way ANOVA was performed at 03:00 and 06:00 for cyto-GCaMP versus cyto-GFP (*$p < 0.05$; **$p < 0.001$). Error bars indicate SEM; *n* represents number of single cells analyzed. Scale bars, 5 μm; timescale = min:sec.

Mitochondria of zebrafish cones are poised to buffer Ca^{2+} from either the cell body or the outer segment

Photoreceptor mitochondria are large (Kim et al., 2005; Masuda et al., 2016) and heterogeneous (Tarboush et al., 2014). Our 3D reconstruction of the ellipsoid region of a zebrafish cone shows that the mitochondrial cluster consists of ~80 tightly packed mitochondria extending nearly to the plasma membrane. This type of structure could act as a physical barrier that restricts flow of ions between the cell body and outer segment; our findings support this idea. We demonstrate that mitochondrial Ca^{2+} levels increase when we increase either outer segment or cell body $[Ca^{2+}]_i$ selectively and that this transfer of Ca^{2+} into mitochondria is at least partially mediated by the MCU. Blocking MCU activity reduced the ability of cone mitochondria to buffer Ca^{2+} and led to a redistribution of cytosolic Ca^{2+} throughout the cell.

The MCU is a complex consisting of the pore-forming MCU subunit and a number of Ca^{2+}-sensitive regulatory proteins that tightly control Ca^{2+} uptake into mitochondria (for review, see Kamer and Mootha, 2015). This protein complex is thought to be the primary route by which Ca^{2+} enters mitochondria and, when it is knocked out, Ca^{2+} uptake into mitochondria is greatly reduced (Pan et al., 2013). From studies in other tissues, the affinity of the MCU for Ca^{2+} appears weak, reported to be between 10 and 25 μM $[Ca^{2+}]_i$ (Gunter and Gunter, 2001; Williams et al., 2013). Expression of activating and deactivating MCU subunits can influence MCU activity and varies widely among cell types (Geiger et al., 2013; Murgia and Rizzuto, 2015), but the stoichiometry of these key regulators in the photoreceptor MCU complex is not known.

ER may facilitate Ca^{2+} uptake into cone mitochondria facing the cell body

In many cell types, a dynamic and extensive network of ER-mitochondrial contacts enables mitochondrial Ca^{2+} uptake by concentrating Ca^{2+} at these junctions (Hamasaki et al., 2013; Rutter and Pinton, 2014). IP_3 receptors on the ER surface release Ca^{2+} immediately adjacent to mitochondria (Rowland and Voeltz, 2012), generating high localized Ca^{2+} concentrations. Ca^{2+} then passes through voltage-dependent anion channels in the outer mitochondrial membrane, generating domains of high $[Ca^{2+}]_i$ that are sufficient for activation of the MCU (Contreras et al., 2010; Qi et al., 2015).

We found that the ER of zebrafish cones surrounds only the basal and lateral parts of the mitochondrial cluster, but does not appear to penetrate the cluster or extend between the apical side and outer segment. This finding is generally consistent with a previous analysis of ER in amphibian cones (Mercurio and

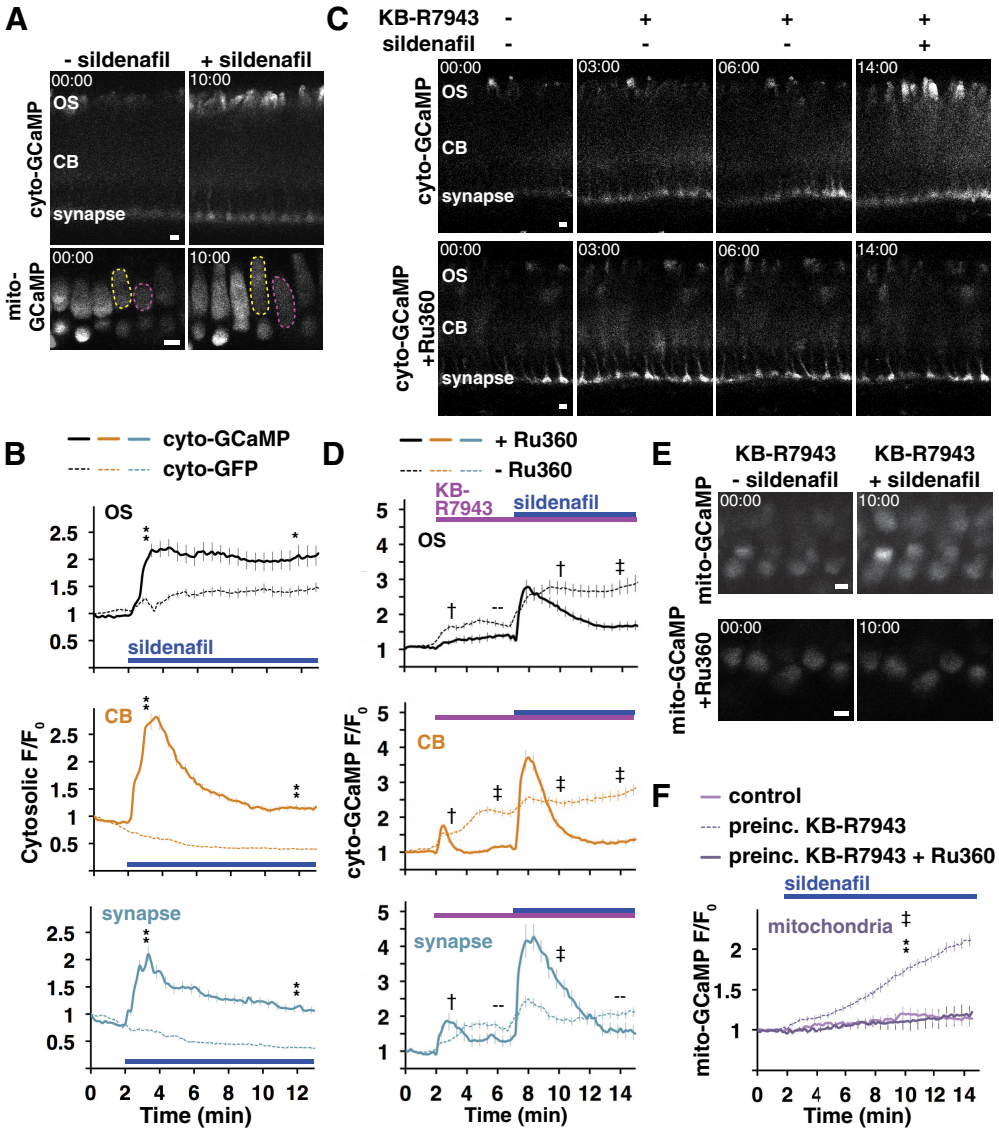

Figure 6. Cone mitochondria buffer Ca^{2+} from the outer segment. ***A***, Representative confocal image of *in situ* retinal slices from transgenic dark-adapted zebrafish expressing GCaMP in cones before (left) and after (right) treatment with 25 μM sildenafil. Top, cyto-GCaMP; bottom, mito-GCaMP with two cone ellipsoids outlined. ***B***, Mean fluorescence responses of single cone outer segment (OS) (top), cell body (CB) (middle), and synapses (bottom) during sildenafil treatment. Solid lines, cyto-GCaMP (5 experiments; *n* for OS = 39, CB = 48, synapses = 50); dashed lines, cyto-GFP control (2 experiments; *n* for OS = 20, CB = 20, synapses = 20); blue bars, presence of 25 μM sildenafil. One-way ANOVA was performed at 03:00 and 12:00 for cyto-GCaMP v cyto-GFP; $*p < 0.05$, $**p < 0.001$. ***C***, Confocal image montages of cone cyto-GCaMP-expressing retinal slices during sequential treatment with 100 μM KB-R7943, then 25 μM sildenafil. Top, Control. Bottom, Ru360 preincubation. ***D***, Mean cyto-GCaMP responses of single cone OS (top), CB (middle), and synapses (bottom) during sildenafil treatment. Solid lines, Ru360 preincubation (3 experiments; *n* for OS = 40, CB = 38, synapses = 29); dashed lines, control (6 experiments; *n* for OS = 65, CB = 69, synapses = 75); magenta bars, presence of 100 μM KB-R7943; blue bars, presence of 25 μM sildenafil. One-way ANOVA was performed at 03:00, 06:00, 10:00, and 14:00 for cyto-GCaMP control versus cyto-GCaMP Ru360; $\dagger p < 0.05$, $\ddagger p < 0.001$. ***E***, Representative confocal images of cone mito-GCaMP expressing retinal slices preincubated in KB-R7943 before (left) and after (right) treatment with 25 μM sildenafil. Top, mito-GCaMP control. Bottom, mito-GCaMP with additional Ru360 preincubation. ***F***, Mean mito-GCaMP responses from mitochondrial clusters of single cones during sildenafil treatment. Solid light lines, control (6 experiments; $n = 60$ cells); dashed lines, KB-R7943 preincubation (5 experiments; $n = 76$ cells); solid dark lines, combined KB-R7943 and Ru360 preincubation (3 experiments; $n = 30$ cells); magenta bars, presence of 100 μM KB-R7943; blue bars, presence of 25 μM sildenafil. One-way ANOVA was performed at 03:00 and 10:00 for mito-GCaMP control versus KB-R7943 pretreatment ($**p < 1 \times 10^{-5}$) and mito-GCaMP KB-R7943 pretreatment versus KB-R7943 with Ru360 pretreatment ($\ddagger p < 1 \times 10^{-5}$). Error bars indicate SEM; *n* represents number of single cells analyzed. Scale bars, 5 μm; timescale = min:sec.

Holtzman, 1982). For the subset of cone mitochondria facing the cell body, where $[Ca^{2+}]_i$ is tens of nanomoles, Ca^{2+} uptake likely occurs at or near ER contact sites. Consistent with this, when we depolarized cones with KCl or block ER Ca^{2+} uptake via SERCA, there was no effect on outer segment $[Ca^{2+}]_i$, whereas synaptic, inner segment, and mitochondrial Ca^{2+} levels increased. Further, recent work showed that Ca^{2+} moves freely through the ER, enabling bidirectional flow of Ca^{2+} between the cell body and the synapse (Chen et al., 2015). This would provide a potential route for synaptic Ca^{2+} to enter mitochondria via MCU.

Mitochondrial Ca^{2+} uptake insulates the cell body from high outer segment $[Ca^{2+}]_i$

The physiological range of free $[Ca^{2+}]_i$ in the outer segment under peak signaling conditions is in the range of tens to hundreds of nanomoles (Krizaj and Copenhagen, 2002), below the affinity of MCU. In addition, plasma membrane Ca^{2+} extrusion from the outer segment via NCKX is significantly faster than extrusion of Ca^{2+} out of the cell body via NCX or PMCA (Krizaj and Copenhagen, 1998). This would suggest that, under normal physiological conditions, outer segment Ca^{2+} is removed pri-

marily through outer segment NCKX (Krizaj and Copenhagen, 2002) and may not depend on mitochondrial Ca^{2+} buffering. Our results suggest that mitochondria mediate high outer segment $[Ca^{2+}]_i$ that might occur during photoreceptor disease.

We found a large capacity for mitochondrial Ca^{2+} buffering under pharmacological conditions that both blocked Ca^{2+} extrusion and forced outer segment Ca^{2+} influx to mimic darkness. These conditions elicited an outer segment $[Ca^{2+}]_i$ increase that approached saturation of our cytosolic Ca^{2+} sensor and increased fluorescence of the mitochondrial Ca^{2+} sensor nearly twofold, the largest change seen in this study. Higher-resolution imaging methods and detailed information about MCU localization across the mitochondrial cluster are needed to address whether outer segment Ca^{2+} enters mitochondria directly near the base of the ciliary stalk or must first diffuse laterally toward the ER to be taken up into mitochondria.

Course of retinal degeneration could be influenced by mitochondrial Ca^{2+} uptake

Our results suggest that mitochondrial Ca^{2+} buffering plays an integral role in photoreceptor survival during degenerations marked by elevated outer segment $[Ca^{2+}]_i$. The *pde6c*^{w59} zebrafish model, which lacks cone PDE6 (Stearns et al., 2007), undergoes retinal degeneration that was predicted to occur via increased cytosolic $[Ca^{2+}]_i$. Interestingly, cytosolic $[Ca^{2+}]_i$ was not increased during cell death (Ma et al., 2013) and our results suggest that elevated outer segment $[Ca^{2+}]_i$ brought on by the mutation may have been buffered by mitochondria. Examination of Ca^{2+} uptake by mitochondria in retinal disease models will define the contributions of mitochondrial Ca^{2+} buffering to disease progression and degeneration.

Photoreceptors of *Nckx1*$^{-/-}$ mice, which lack rod outer segment NCKX, degenerate very slowly, showing thinning of retinal layers over the course of a year (Vinberg et al., 2015). These mice exhibit a delayed recovery of rod photoresponse. Absent an efflux route at the plasma membrane, Ca^{2+} can still slowly leave the outer segment. A recent study of *Nckx2*$^{-/-}$ mice lacking cone outer segment NCKX demonstrated a similar delay in recovery of cone photoresponse, but cones do not degenerate (Sakurai et al., 2016). Together, these studies are consistent with a previous observation that cone mitochondria may have more Ca^{2+}-buffering capacity than rods (Szikra and Krizaj, 2007). We found that cone mitochondria can accumulate Ca^{2+} via MCU, which could contribute to photoresponse recovery in these mutants. Knock-out models lacking the MCU and modulators of mitochondrial Ca^{2+} uptake will help to determine whether Ca^{2+} uptake by mitochondria influences photoresponse recovery.

In summary, cone photoreceptor mitochondria can influence $[Ca^{2+}]_i$ in the cell body and outer segment. This is important for isolating functional information within distinct photoreceptor compartments. Ca^{2+} buffered by mitochondria located on the cell body side of the cluster may regulate protein synthesis and metabolic processes through protein acetylation and NADH production. Mitochondrial Ca^{2+} buffering from the outer segment may be a small but important component of light adaptation because recovery of photocurrent after sustained increases in light could be influenced by mitochondrial uptake of outer segment Ca^{2+}. Ca^{2+} buffering via mitochondria could also influence the health and survival of photoreceptors during degeneration due to disease-causing mutations. Future studies should evaluate the contributions of mitochondrial Ca^{2+} import to photoreceptor metabolism, light adaptation, and disease.

References

Augustine GJ, Santamaria F, Tanaka K (2003) Local calcium signaling in neurons. Neuron 40:331–346. CrossRef Medline

Baughman JM, Perocchi F, Girgis HS, Plovanich M, Belcher-Timme CA, Sancak Y, Bao XR, Strittmatter L, Goldberger O, Bogorad RL, Koteliansky V, Mootha VK (2011) Integrative genomics identifies MCU as an essential component of the mitochondrial calcium uniporter. Nature 476:341–345. CrossRef Medline

Beckers CJ, Balch WE (1989) Calcium and GTP: essential components in vesicular trafficking between the endoplasmic reticulum and Golgi apparatus. J Cell Biol 108:1245–1256. CrossRef Medline

Booth C, Koch GL (1989) Perturbation of cellular calcium induces secretion of luminal ER proteins. Cell 59:729–737. CrossRef Medline

Burnside B, Wang E, Pagh-Roehl K, Rey H (1993) Retinomotor movements in isolated teleost retinal cone inner-outer segment preparations (CIS-COS): effects of light, dark and dopamine. Exp Eye Res 57:709–722. CrossRef Medline

Chen M, Van Hook MJ, Thoreson WB (2015) Ca^{2+} diffusion through endoplasmic reticulum supports elevated intraterminal Ca^{2+} levels needed to sustain synaptic release from rods in darkness. J Neurosci 35:11364–11373. CrossRef Medline

Contreras L, Drago I, Zampese E, Pozzan T (2010) Mitochondria: the calcium connection. Biochim Biophys Acta 1797:607–618. CrossRef Medline

De Stefani D, Raffaello A, Teardo E, Szabò I, Rizzuto R (2011) A forty-kilodalton protein of the inner membrane is the mitochondrial calcium uniporter. Nature 476:336–340. CrossRef Medline

Dizhoor AM (2000) Regulation of cGMP synthesis in photoreceptors: role in signal transduction and congenital diseases of the retina. Cell Signal 12:711–719. CrossRef Medline

Dowling JE (1987) The retina: an approachable part of the brain. Cambridge, MA: Harvard University.

Du J, Cleghorn W, Contreras L, Linton JD, Chan GC, Chertov AO, Saheki T, Govindaraju V, Sadilek M, Satrústegui J, Hurley JB (2013) Cytosolic reducing power preserves glutamate in retina. Proc Natl Acad Sci U S A 110:18501–18506. CrossRef Medline

Du J, Rountree A, Cleghorn WM, Contreras L, Lindsay KJ, Sadilek M, Gu H, Djukovic D, Raftery D, Satrústegui J, Kanow M, Chan L, Tsang SH, Sweet IR, Hurley JB (2016) Phototransduction influences metabolic flux and nucleotide metabolism in mouse retina. J Biol Chem 291:4698–4710. CrossRef Medline

Esterberg R, Hailey DW, Rubel EW, Raible DW (2014) ER-mitochondrial calcium flow underlies vulnerability of mechanosensory hair cells to damage. J Neurosci 34:9703–9719. CrossRef Medline

Fox J (2005) The R commander: a basic-statistics graphical user interface to R. Journal of Statistical Software 14:1–42.

Geiger T, Velic A, Macek B, Lundberg E, Kampf C, Nagaraj N, Uhlen M, Cox J, Mann M (2013) Initial quantitative proteomic map of 28 mouse tissues using the SILAC mouse. Mol Cell Proteomics 12:1709–1722. CrossRef Medline

George AA, Hayden S, Holzhausen LC, Ma EY, Suzuki SC, Brockerhoff SE (2014) Synaptojanin 1 is required for endolysosomal trafficking of synaptic proteins in cone photoreceptor inner segments. PLoS One 9:e84394. CrossRef Medline

Glancy B, Balaban RS (2012) Role of mitochondrial Ca^{2+} in the regulation of cellular energetics. Biochemistry 51:2959–2973. CrossRef Medline

Glancy B, Hartnell LM, Malide D, Yu ZX, Combs CA, Connelly PS, Subramaniam S, Balaban RS (2015) Mitochondrial reticulum for cellular energy distribution in muscle. Nature 523:617–620. CrossRef Medline

Gorczyca WA, Polans AS, Surgucheva IG, Subbaraya I, Baehr W, Palczewski K (1995) Guanylyl cyclase activating protein: a calcium-sensitive regulator of phototransduction. J Biol Chem 270:22029–22036. CrossRef Medline

Greenawalt JW, Rossi CS, Lehninger AL (1964) Effect of active accumulation of calcium and phosphate ions on the structure of rat liver mitochondria. J Cell Biol 23:21–38. CrossRef Medline

Gunter TE, Gunter KK (2001) Uptake of calcium by mitochondria: transport and possible function. IUBMB Life 52:197–204. CrossRef Medline

Hamasaki M, Furuta N, Matsuda A, Nezu A, Yamamoto A, Fujita N, Oomori H, Noda T, Haraguchi T, Hiraoka Y,Amano A, Yoshimori T (2013) Autophagosomes form at ER-mitochondria contact sites. Nature 495:389–393. CrossRef Medline

Heidelberger R, Thoreson WB, Witkovsky P (2005) Synaptic transmission

at retinal ribbon synapses. Progress in Retinal and Eye Research 24:682–720. CrossRef Medline

Iwamoto T, Watano T, Shigekawa M (1996) A novel isothiourea derivative selectively inhibits the reverse mode of Na^+/Ca^{2+} exchange in cells expressing NCX1. J Biol Chem 271:22391–22397. CrossRef Medline

Johnson JE Jr, Perkins GA, Giddabasappa A, Chaney S, Xiao W, White AD, Brown JM, Waggoner J, Ellisman MH, Fox DA (2007) Spatiotemporal regulation of ATP and Ca^{2+} dynamics in vertebrate rod and cone ribbon synapses. Mol Vis 13:887–919. Medline

Jouaville LS, Pinton P, Bastianutto C, Rutter GA, Rizzuto R (1999) Regulation of mitochondrial ATP synthesis by calcium: evidence for a long-term metabolic priming. Proc Natl Acad Sci U S A 96:13807–13812. CrossRef Medline

Kamer KJ, Mootha VK (2015) The molecular era of the mitochondrial calcium uniporter. Nat Rev Mol Cell Biol 16:545–553. CrossRef Medline

Kawamura S, Murakami M (1991) Calcium-dependent regulation of cyclic GMP phosphodiesterase by a protein from frog retinal rods. Nature 349:420–423. CrossRef Medline

Kennedy BN, Alvarez Y, Brockerhoff SE, Stearns GW, Sapetto-Rebow B, Taylor MR, Hurley JB (2007) Identification of a zebrafish cone photoreceptor-specific promoter and genetic rescue of achromatopsia in the nof mutant. Invest Ophthalmol Vis Sci 48:522–529. CrossRef Medline

Kim J, Lee E, Chang BS, Oh CS, Mun GH, Chung YH, Shin DH (2005) The presence of megamitochondria in the ellipsoid of photoreceptor inner segment of the zebrafish retina. Anat Histol Embryol 34:339–342. CrossRef Medline

Kirichok Y, Krapivinsky G, Clapham DE (2004) The mitochondrial calcium uniporter is a highly selective ion channel. Nature 427:360–364. CrossRef Medline

Kourennyi DE, Barnes S (2000) Depolarization-induced calcium channel facilitation in rod photoreceptors Is independent of G proteins and phosphorylation. J Neurophysiol 84:133–138. Medline

Krizaj D, Copenhagen DR (1998) Compartmentalization of calcium extrusion mechanisms in the outer and inner segments of photoreceptors. Neuron 21:249–256. CrossRef Medline

Krizaj D, Copenhagen DR (2002) Calcium regulation in photoreceptors. Front Biosci 7:d2023–d2044. Medline

Krizaj D, Demarco SJ, Johnson J, Strehler EE, Copenhagen DR (2002) Cell-specific expression of plasma membrane calcium ATPase isoforms in retinal neurons. J Comp Neurol 451:1–21. CrossRef Medline

Kwan KM, Fujimoto E, Grabher C, Mangum BD, Hardy ME, Campbell DS, Parant JM, Yost HJ, Kanki JP, Chien CB (2007) The Tol2kit: a multisite gateway-based construction kit forTol2 transposon transgenesis constructs. Dev Dyn 236:3088–3099. CrossRef Medline

Kwong JQ, Lu X, Correll RN, Schwanekamp JA, Vagnozzi RJ, Sargent MA, York AJ, Zhang J, Bers DM, Molkentin JD (2015) The mitochondrial calcium uniporter selectively matches metabolic output to acute contractile stress in the heart. Cell Reports 12:15–22. CrossRef Medline

Lee A, Wang S, Williams B, Hagen J, Scheetz TE, Haeseleer F (2015) Characterization of CaV1.4 complexes (α_1 1.4, β_2, and $\alpha_2\delta_4$) in HEK293T cells and in the retina. J Biol Chem 290:1505–1521. CrossRef Medline

Llorente-Folch I, Rueda CB, Amigo I, del Arco A, Saheki T, Pardo B, Satrústegui J (2013) Calcium-regulation of mitochondrial respiration maintains ATP homeostasis and requires ARALAR/AGC1-malate aspartate shuttle in intact cortical neurons. J Neurosci 33:13957–13971, 13971a. CrossRef Medline

Lytton J, Westlin M, Hanley MR (1991) Thapsigargin inhibits the sarcoplasmic or endoplasmic reticulum Ca-ATPase family of calcium pumps. J Biol Chem 266:17067–17071. Medline

Ma EY, Lewis A, Barabas P, Stearns G, Suzuki S, Krizaj D, Brockerhoff SE (2013) Loss of Pde6 reduces cell body Ca^{2+} transients within photoreceptors. Cell Death Dis 4:e797. CrossRef Medline

MacAskill AF, Rinholm JE, Twelvetrees AE, Arancibia-Carcamo IL, Muir J, Fransson A, Aspenstrom P, Attwell D, Kittler JT (2009) Miro1 Is a calcium sensor for glutamate receptor-dependent localization of mitochondria at synapses. Neuron 61:541–555. CrossRef Medline

Mammucari C, Gherardi G, Zamparo I, Raffaello A, Boncompagni S, Chemello F, Cagnin S, Braga A, Zanin S, Pallafacchina G, Zentilin L, Sandri M, De Stefani D, Protasi F, Lanfranchi G, Rizzuto R (2015) The mitochondrial calcium uniporter controls skeletal muscle trophism in vivo. Cell Reports 10:1269–1279. CrossRef Medline

Marcu R, Wiczer BM, Neeley CK, Hawkins BJ (2014) Mitochondrial matrix Ca^{2+} accumulation regulates cytosolic NAD^+/NADH metabolism, protein acetylation, and sirtuin expression. Mol Cell Biol 34:2890–2902. CrossRef Medline

Masuda T, Wada Y, Kawamura S (2016) ES1 is a mitochondrial enlarging factor contributing to form mega-mitochondria in zebrafish cones. Sci Rep 6:22360. CrossRef Medline

Matlib MA, Zhou Z, Knight S, Ahmed S, Choi KM, Krause-Bauer J, Phillips R, Altschuld R, Katsube Y, Sperelakis N, Bers DM (1998) Oxygen-bridged dinuclear ruthenium amine complex specifically inhibits Ca^{2+} uptake into mitochondria in vitro and in situ in single cardiac myocytes. J Biol Chem 273:10223–10231. CrossRef Medline

Mercurio AM, Holtzman E (1982) Smooth endoplasmic reticulum and other agranular reticulum in frog retinal photoreceptors. J Neurocytol 11:263–293. CrossRef Medline

Murgia M, Rizzuto R (2015) Molecular diversity and pleiotropic role of the mitochondrial calcium uniporter. Cell Calcium 58:11–17. CrossRef Medline

Pan X, Liu J, Nguyen T, Liu C, Sun J, Teng Y, Fergusson MM, Rovira II, Allen M, Springer DA, Aponte AM, Gucek M, Balaban RS, Murphy E, Finkel T (2013) The physiological role of mitochondrial calcium revealed by mice lacking the mitochondrial calcium uniporter. Nat Cell Biol 15:1464–1472. CrossRef Medline

Qi H, Li L, Shuai J (2015) Optimal microdomain crosstalk between endoplasmic reticulum and mitochondria for Ca^{2+} oscillations. Sci Rep 5:7984. CrossRef Medline

Qiu J, Tan YW, Hagenston AM, Martel MA, Kneisel N, Skehel PA, Wyllie DJ, Bading H, Hardingham GE (2013) Mitochondrial calcium uniporter MCU controls excitotoxicity and is transcriptionally repressed by neuroprotective nuclear calcium signals. Nat Commun 4:2034. Medline

Rieke F, Schwartz EA (1996) Asynchronous transmitter release: control of exocytosis and endocytosis at the salamander rod synapse. J Physiol 493:1–8. Medline

Rowland AA, Voeltz GK (2012) Endoplasmic reticulum–mitochondria contacts: function of the junction. Nat Rev Mol Cell Biol 13:607–625. CrossRef Medline

Rutter GA, Pinton P (2014) Mitochondria-associated endoplasmic reticulum membranes in insulin signaling. Diabetes 63:3163–3165. CrossRef Medline

Sakurai K, Vinberg F, Wang T, Chen J, Kefalov VJ (2016) The Na^+/Ca^{2+}, K^+ exchanger 2 modulates mammalian cone phototransduction. Sci Rep 6:32521. CrossRef Medline

Sampath AP, Matthews HR, Cornwall MC, Bandarchi J, Fain GL (1999) Light-dependent changes in outer segment free-Ca^{2+} concentration in salamander cone photoreceptors. J Gen Physiol 113:267–277. CrossRef Medline

Satrústegui J, Pardo B, Del Arco A (2007) Mitochondrial transporters as novel targets for intracellular calcium signaling. Physiol Rev 87:29–67. CrossRef Medline

Schmitz F (2014) Presynaptic [Ca^{2+}] and GCAPs: aspects on the structure and function of photoreceptor ribbon synapses. Front Mol Neurosci 7:3. CrossRef Medline

Schnetkamp PP, Szerencsei RT, Basu DK (1991) Unidirectional Na^+, Ca^{2+}, and K^+ fluxes through the bovine rod outer segment Na-Ca-K exchanger. J Biol Chem 266:198–206. Medline

Stearns G, Evangelista M, Fadool JM, Brockerhoff SE (2007) A mutation in the cone-specific pde6 gene causes rapid cone photoreceptor degeneration in zebrafish. J Neurosci 27:13866–13874. CrossRef Medline

Szikra T, Krizaj D (2007) Intracellular organelles and calcium homeostasis in rods and cones. Vis Neurosci 24:733–743. CrossRef Medline

Tarboush R, Chapman GB, Connaughton VP (2012) Ultrastructure of the distal retina of the adult zebrafish, *Danio rerio*. Tissue Cell 44:264–279. CrossRef Medline

Tarboush R, Novales Flamarique I, Chapman GB, Connaughton VP (2014) Variability in mitochondria of zebrafish photoreceptor ellipsoids. Vis Neurosci 31:11–23. CrossRef Medline

Taylor WR, Morgans C (1998) Localization and properties of voltage-gated calcium channels in cone photoreceptors of *Tupaia belangeri*. Vis Neurosci 15:541–552. Medline

Thoreson WB, Rabl K, Townes-Anderson E, Heidelberger R (2004) A highly Ca^{2+}-sensitive pool of vesicles contributes to linearity at the rod photoreceptor ribbon synapse. Neuron 42:595–605. CrossRef Medline

Vinberg F, Wang T, Molday RS, Chen J, Kefalov VJ (2015) A new mouse

model for stationary night blindness with mutant Slc24a1 explains the pathophysiology of the associated human disease. Hum Mol Genet 24: 5915–5929. CrossRef Medline

Wan B, LaNoue KF, Cheung JY, Scaduto RC Jr (1989) Regulation of citric acid cycle by calcium. J Biol Chem 264:13430–13439. Medline

Wang C, Xie N, Wang Y, Li Y, Ge X, Wang M (2015) Role of the Mitochondrial Calcium Uniporter in rat hippocampal neuronal death after pilocarpine-induced status epilepticus. Neurochem Res 40:1739–1746. CrossRef Medline

Wang W, Fang H, Groom L, Cheng A, Zhang W, Liu J, Wang X, Li K, Han P, Zheng M, Yin J, Wang W, Mattson MP, Kao JP, Lakatta EG, Sheu SS, Ouyang K, Chen J, Dirksen RT, Cheng H (2008) Superoxide flashes in single mitochondria. Cell 134:279–290. CrossRef Medline

Wiczer BM, Marcu R, Hawkins BJ (2014) KB-R7943, a plasma membrane Na^+/Ca^{2+} exchanger inhibitor, blocks opening of the mitochondrial permeability transition pore. Biochem Biophys Res Commun 444:44–49. CrossRef Medline

Williams GS, Boyman L, Chikando AC, Khairallah RJ, Lederer WJ (2013) Mitochondrial calcium uptake. Proc Natl Acad Sci U S A 110:10479–10486. CrossRef Medline

Yang HH, St-Pierre F, Sun X, Ding X, Lin MZ, Clandinin TR (2016) Subcellular imaging of voltage and calcium signals reveals neural processing in vivo. Cell 166:245–257. CrossRef Medline

Zenisek D, Matthews G (2000) The role of mitochondria in presynaptic calcium handling at a ribbon synapse. Neuron 25:229–237. CrossRef Medline

Zhang X, Feng Q, Cote RH (2005) Efficacy and selectivity of phosphodiesterase-targeted drugs in inhibiting photoreceptor phosphodiesterase (PDE6) in retinal photoreceptors. Investigative Ophthalmology and Visual Science 46:3060–3066. CrossRef Medline